ADVANCED HEALTHCARE MATERIALS
www.advhealthmat.de

Sustained Delivery of SARS-CoV-2 RBD Subunit Vaccine Using a High Affinity Injectable Hydrogel Scaffold

Jing Chen, Bo Wang, Julia S. Caserto, Kaavian Shariati, Peng Cao, Yang Pan, Qixuan Xu, and Minglin Ma**

The receptor binding domain (RBD) of severe acute respiratory syndrome coronavirus 2 (SARS-CoV-2) spike protein that mediates viral entry into host cells is a good candidate immunogen for vaccine development against coronavirus disease 2019 (COVID-19). Because of its small size, most preclinical and early clinical efforts have focused on multimerizing RBD on various formats of nanoparticles to increase its immunogenicity. Using an easily administered injectable hydrogel scaffold that is rationally designed for enhanced retainment of RBD, an alternative and facile approach for boosting RBD immunogenicity in mice is demonstrated. Prolonged delivery of poly (I:C) adjuvanted RBD by the hydrogel scaffold results in sustained exposure to lymphoid tissues, which elicits serum IgG titers comparable to those induced by three bolus injections, but more long-lasting and polarized toward T_H1-mediated IgG2b. The hydrogel scaffold induces potent germinal center (GC) reactions, correlating with RBD-specific antibody generation and robust type 1 T cell responses. Besides being an enduring RBD reservoir, the hydrogel scaffold becomes a local inflammatory niche for innate immune cell activation. Collectively, the injectable hydrogel scaffold provides a simple, practical, and inexpensive means to enhance the efficacy of RBD-based subunit vaccines against COVID-19 and may be applicable to other circulating and emerging pathogens.

1. Introduction

The rapid spread of coronavirus disease 2019 (COVID-19) has caused devastating health and economic impacts worldwide.[1,2] Over 205 million confirmed cases, including more than 4.3 million deaths, are reported as of early August 2021 (https://covid19.who.int/). Although multiple vaccines were developed and emergently authorized to mitigate the high morbidity and mortality of COVID-19,[3,4] challenges remain. For example, mRNA vaccines are unstable are rely strongly on cold chain logistics,[5] inactivated virus vaccines require strict manufacturing conditions,[6,7] and recombinant adenovirus vaccines are found to induce rare but severe side effects.[8,9] On the other hand, subunit vaccines may provide an alternative due to better stability, easier manufacture, and lower cost.[10] The receptor binding domain (RBD) of the syndrome coronavirus 2 (SARS-CoV-2) spike protein is a good candidate for subunit vaccine development owing to its role in virus entry by interacting with angiotensin-converting enzyme 2 (ACE2) receptors on host cells.[2] Therefore, SARS-CoV-2 RBD immunization can induce specific neutralizing antibodies which could block this recognition and thus effectively prevent invasion of the virus.

However, due to its small size, SARS-CoV-2 RBD is poorly immunogenic; it often requires the use of an adjuvant, or multimerization of RBD to boost its efficacy.[5,10–13] Moreover, both the RBD and the adjuvant suffer from short half-life after administration due to rapid systemic clearance. Unlike natural infections, the short duration of antigen exposure is often insufficient to elicit a potent humoral immune response, which requires an orchestrated immune cascade involving antigen-presenting cell (APC) activation, T cell priming, and germinal center (GC) reactions in secondary lymphoid organs. Therefore, to induce high and long-lasting titers of neutralizing antibodies, most vaccines require one or more booster shots after primary injection. The costly and inconvenient dosing processes significantly increase the burden to those being vaccinated, particularly those in remote or underdeveloped areas, which greatly hinders the establishment of a powerful immunological barrier.

Hydrogels, because of their high water content,[14,15] tunable mechanical properties,[16,17] and good biocompatibility,[18,19] have shown great promise in developing drug delivery systems for cardiovascular diseases,[20–22] malignant tumors,[23,24] and diabetes.[25–27] In terms of vaccination applications, viral

P. Cao, Y. Pan, Q. Xu
College of Pharmacy
Nanjing University of Chinese Medicine
Nanjing 210023, China
J. Chen, B. Wang, K. Shariati, M. Ma
Department of Biological and Environmental Engineering
Cornell University
Ithaca, NY 14853, USA
E-mail: bw454@cornell.edu; mm826@cornell.edu
J. S. Caserto
Robert Frederick Smith School of Chemical and Biomolecular Engineering
Cornell University
Ithaca, NY 14853, USA
The ORCID identification number(s) for the author(s) of this article can be found under https://doi.org/10.1002/adhm.202101714

DOI: 10.1002/adhm.202101714

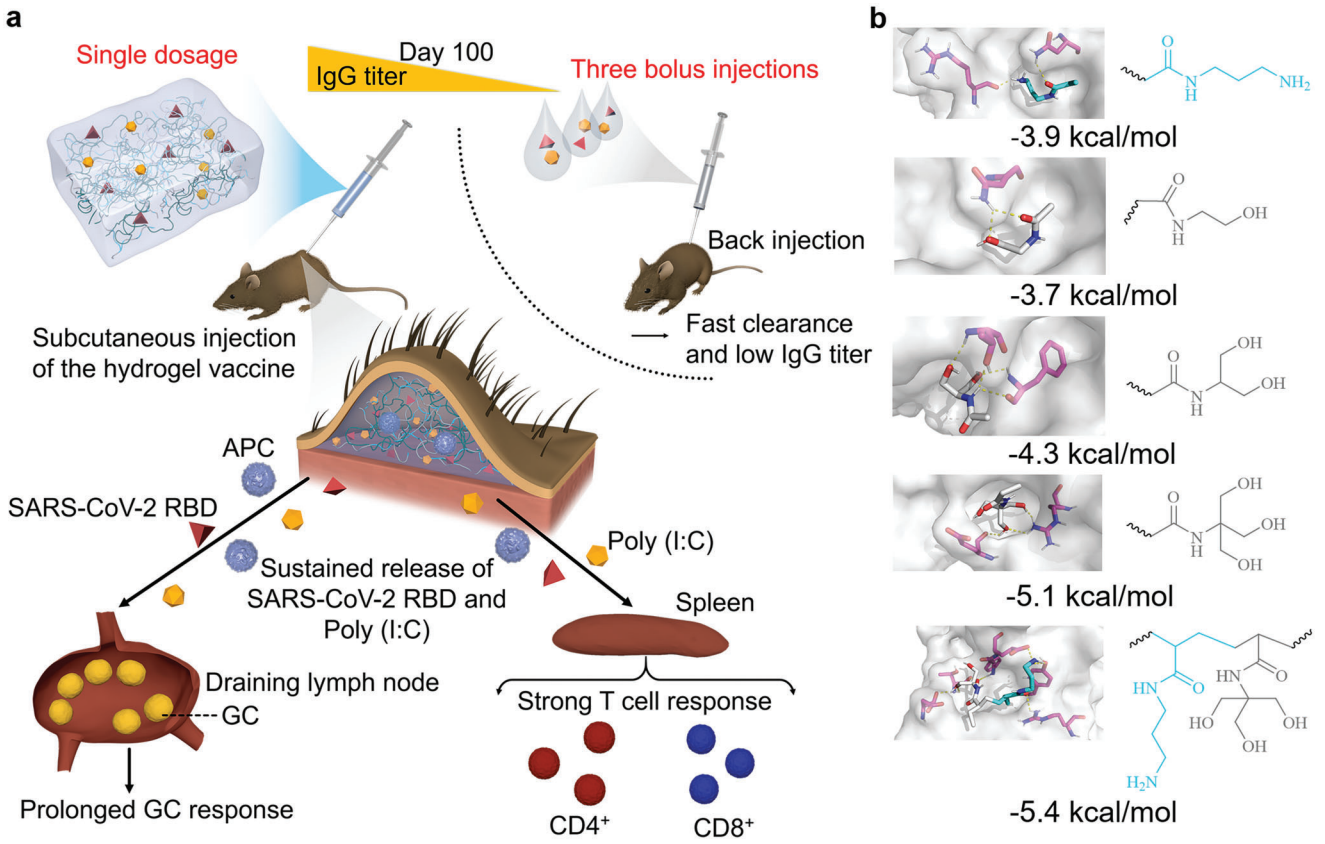

Figure 1. Schematic and selection of the high affinity injectable hydrogel scaffold for RBD and poly (I:C) loading. a) Scheme of the injectable hydrogel for sustained delivery of SARS-CoV-2 RBD and poly(I:C). b) Affinities of SARS-CoV-2 RBD with various polymer side chains: APMA, single hydroxyl group functionalized, two hydroxyl group functionalized, THMA and APMA-THMA.

antigens and 3-*O*-desacyl-4′-monophosphoryl lipid A co-loaded in poly(γ-glutamic acid)/collagen hydrogels induced 3.36 times higher antigen-specific IgG titers compared to those without hydrogel encapsulation after two weeks of intramuscular immunization.[28] Injectable polymer-nanoparticle composite hydrogels were used to co-deliver ovalbumin and poly(I:C) and achieved prolonged humoral immune responses,[29] however, the antibody titer of hydrogel group rapidly dropped after 40 days. A mesoporous silica micro-rod vaccine system was developed to elicit stronger titers of antibody than one bolus injection over 12 months.[30] Despite these promising developments, it is still challenging to generate durable immune responses that can match or outperform multiple bolus injections. If successful, such a system could potentially advance vaccination by reducing cost.

Here, we report a high affinity injectable hydrogel scaffold for sustained delivery of poly (I:C) adjuvanted SARS-CoV-2 RBD as a simple and low-cost approach to enhance the potency of RBD-based subunit vaccines (**Figure 1**a). Using multiple immunological assays, we demonstrated that a single administration of the hydrogel vaccine generated a local inflammatory niche for innate immune cell recruitment and activation, which enhanced germinal center (GC) reactions and subsequently resulted in serum IgG titers comparable to those induced by three bolus injections. We also showed that the hydrogel formulation elicited robust type 1 T cell responses, an important effector arm for protection against COVID-19. Therefore, our injectable hydrogel scaffold may provide an easy-to-deploy means of vaccination against SARS-CoV-2.

2. Results and Discussion

It is known that sustained exposure of an immunogen to lymphoid tissues can improve the immune response and vaccination outcome.[12,29] Therefore, we hypothesized that strong interactions between the hydrogel and the immunogen being delivered would be critical to prolonged release and durable immune responses. We used the Autodock Vina program and crystal structure of SARS-CoV-2 RBD (PDB ID: 7BWJ, E chain) to analyze the affinities between the RBD and different side chain functional groups (Figure 1b). Among the hydrogel chemistries we explored, we identified a poly(N-(3-aminopropyl)methacrylamide)-*co*-(N-[Tris(hydroxymethyl)methyl]acrylamide) (*p*(APMA-THMA)) that contains triple hydrogen bonding clusters[31] and exhibits high affinity to SARS-CoV-2 RBD. The side chain containing both APMA and THMA had lower affinity energy of −5.4 kcal mol^{-1} (i.e., stronger interaction) with the SARS-CoV-2 RBD than that of APMA or THMA alone (−3.9 and −5.1 kcal mol^{-1}, respectively). Meanwhile, single hydroxyl and two hydroxyl groups had affinity energies of −3.7 and −4.3 kcal mol^{-1}, respectively, which were

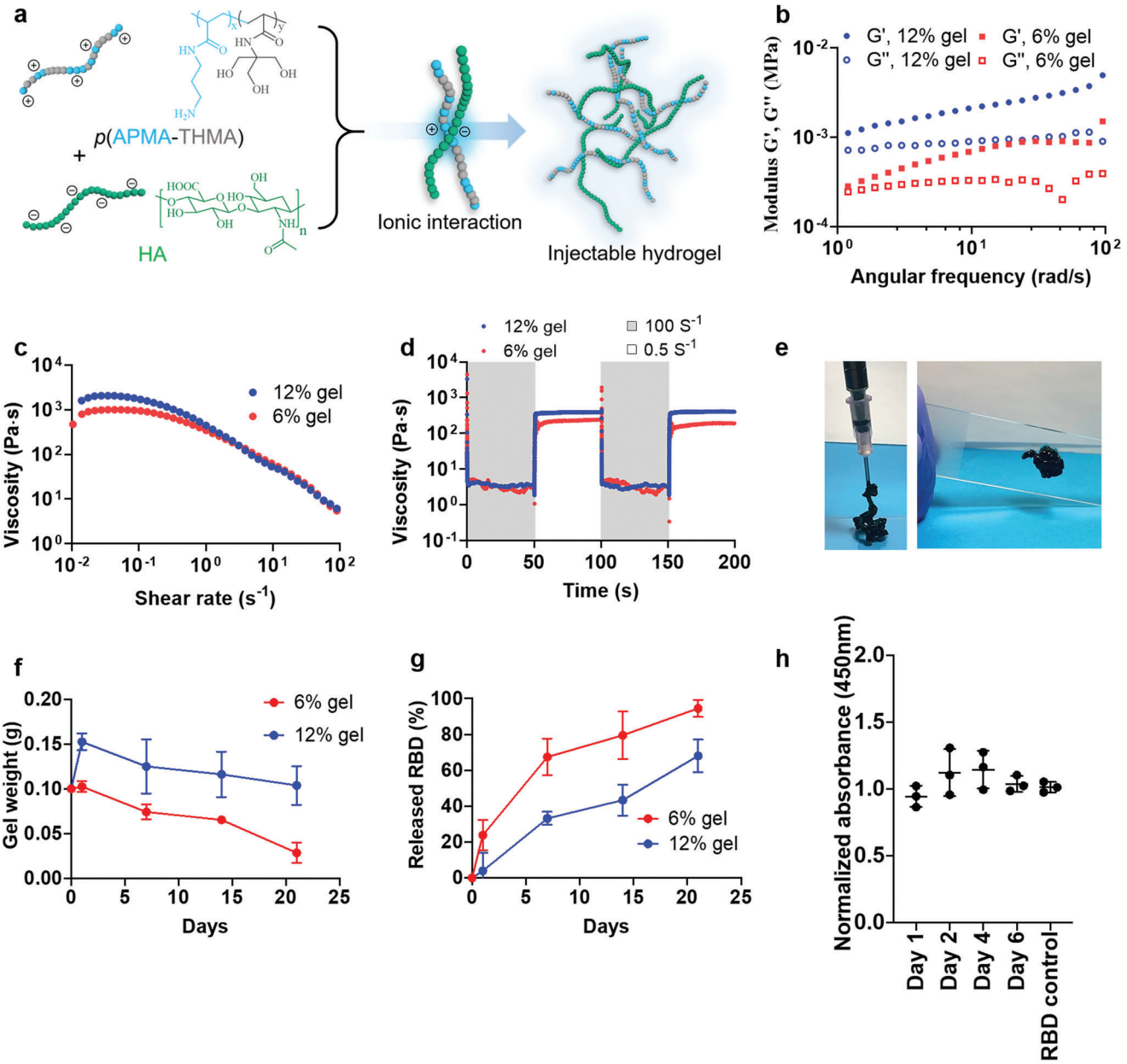

Figure 2. Schematic and characterization of the injectable hydrogel. a) Scheme of the hydrogel preparation. b) Frequency-dependent (strain = 0.1%, 37 °C) oscillatory shear rheology, and c) steady shear rheology of two hydrogel formulations designated as "6% gel" and "12% gel". d) Step-shear measurements of 6% gel and 12% gel over two cycles with alternating high shear (100 s^{-1}) and low shear (0.05 s^{-1}) rates. e) Images of 12% gel injection through an 18-gauge needle during injection (left) and after injection (right) (the hydrogel was mixed with a black food dye for easier visualization). f) In vivo degradation of the hydrogels over time following subcutaneous injection into C57BL/6 mice. g) In vivo RBD release from the hydrogels over time. h) Antigenicity profiles of RBD released from the 12% gel, as evaluated by ELISA analysis with rabbit-anti-RBD polyclonal antibodies. Binding was normalized to released RBD concentration. In (f,g), $n = 3$ mice per group. In (h), $n = 3$ per time point. Mean ± SD was shown.

both higher than the APMA-THMA combination. Interestingly, the binding energy of the APMA-THMA combination was also lower than many of those commonly used side chain of injectable hydrogel materials that have been published for protein delivery (Table S1, Supporting Information), highlighting its strong contact with RBD that may facilitate its sustained delivery.

To develop the *p*(APMA-THMA) into an injectable hydrogel for the RBD delivery, we took advantage of the positive charge of APMA and complexed it with negatively charged hyaluronic acid to form a biodegradable hydrogel through ionic interaction (**Figure 2**a). To adjust the mechanical properties, degradation rates, and RBD release profiles, we chose two hydrogel formulations based on different solid contents (6% and 12% by weight, hereafter termed as 6% gel and 12% gel), which ensured both formation of the hydrogel and its injectability. The rheological properties of the hydrogels were then measured. Frequency-dependent

oscillatory shear experiments, performed in the linear viscoelastic regime, demonstrated a formulation-dependent frequency response (Figure 2b). At a representative angular frequency (ω = 10 rad s^{-1}), the 6% and 12% gels exhibited storage moduli (G') of 689 and 2110 Pa, respectively. An angular frequency sweep showed that hydrogels remained solid-like state, with the G' remaining above the loss modulus (G'') at all frequencies tested. A shear rate sweep showed that the viscosity of these hydrogels decreased over two orders of magnitude with increasing shear rates, thus indicating its injectability (Figure 2c). Injectability was further tested by measuring the viscosity of the hydrogels when alternating between a high shear rate (100 s^{-1}) reminiscent of the injection process and a low shear rate (0.5 s^{-1}) reminiscent of the working conditions upon implantation. The viscosity of both hydrogel formulations decreased by two orders of magnitude with an applied high shear rate and rapidly recovered (<5 s) to their original viscosity when returned to a low shear rate (Figure 2d,e). These data confirmed that the hydrogel scaffolds were injectable and could be loaded with desired cargos.

To determine the in vivo gel degradation and RBD release kinetics, RBD was fluorescently labeled with Cy5 and encapsulated into the two hydrogels (Figure S1, Supporting Information). The formulated hydrogels were injected subcutaneously into C57BL/6 mice and recovered on indicated time points for measurement of residual gel mass and RBD fluorescence. In C57BL/6 mice, the 6% gel degraded faster in comparison with the 12% gel, with ≈ 20% gel mass remaining after 21 days, while the 12% gel had ≈90% gel mass remaining at this time (Figure 2f). Regarding RBD release, the 6% gel released ≈100% encapsulated RBD in 21 days, with a RBD release half-life of 4.6 days, while the 12% gel released ≈70% encapsulated RBD during the same period, with a half-life of 14.1 days (Figure 2g; Figure S2, Supporting Information).

Preservation of structural integrity of the immunogen is a prerequisite for a sustained delivery system for vaccines, as misfolded immunogen may expose unnatural epitopes that elicit futile humoral responses. To confirm the preserved antigenicity of encapsulated RBD in the hydrogel, the 12% gel loaded with RBD was incubated in PBS with mouse serum at 37 °C, and released RBD at different time points was probed by ELISA with rabbit-anti-RBD polyclonal antibodies, which binds various epitopes on RBD and therefore guarantees its structural integrity. Negligible loss in binding was observed in recovered RBD, validating the stability of RBD in the hydrogel (Figure 2h).

We next characterized the in vivo performance of the hydrogel vaccination system. Immune cell infiltration into hydrogels is widely reported, and the infiltrating cells have been demonstrated to be beneficial in certain scenarios, such as T_H2 mediated tissue regeneration.[32,33] For vaccination, sustained delivery of the immunogen from the hydrogel, together with immune cell recruitment into the hydrogel, may synergize to boost the immune responses. Given the biodegradability of the hydrogel scaffolds, we examined whether they caused infiltration of immune cells. 14 days after vaccination, the hydrogel scaffolds were harvested and digested, after which the infiltrating cells were collected and profiled by flow cytometry (Figures S3 and S4 and Table S2, Supporting Information). We found abundant $CD45^+$ immune cells infiltrated into the hydrogel scaffolds (**Figure 3**a). Interestingly, the 12% gel induced infiltration of more cells within each subset, including dendritic cells (DC), macrophages, monocytes, and neutrophils (Figure 3b–e). The increase of infiltrating immune cells, especially APCs, into the 12% gel, probably resulted from the slow degradation of and the slow RBD release from the 12% gel in vivo, which provided a more long-lasting reservoir and antigenic cues for APC recruitment. Among various lymphocyte subsets, neutrophils constituted of the major population, followed by robust numbers of DCs and monocytes. Infiltration of these APCs suggested that the hydrogel scaffolds served as a local inflammatory site for APC priming. We further determined DC subsets in the hydrogel scaffolds. Strikingly, most infiltrated DCs were type 2 conventional DCs (cDC2) (Figure 3f). cDC2 have been demonstrated to prime $CD4^+$ T_{FH} cells and initiate humoral immune responses.[34] Taken together, these results demonstrated that the hydrogel scaffolds provided a special niche for APC activation, which may in turn prime T cells and boost GC reactions in the draining LNs.

We then assessed whether sustained delivery of poly (I:C) adjuvanted RBD using the hydrogel scaffolds could elicit robust RBD-specific humoral immune responses in C57BL/6 mice. Groups of 7–9 mice were immunized with the same total dose of RBD and poly (I:C), formulated in PBS for bolus injections or in the hydrogel scaffolds for slow release (**Figure 4**a). For two and three bolus injections, we adopted a similar interval between injections to be consistent with our previous studies on EBOV VLP and ricin A chain, and with other studies using RBD as immunogen,[11–13,35–37] which should enable more reliable comparison of different vaccine formulations across studies. As antigen-specific serum antibodies usually peak at 10–14 days after immunization, we first analyzed RBD-specific antibody levels 14 days after one bolus (day 14), the final of two bolus (day 28), the final of three bolus (day 42), 6% gel (day 14), and 12% gel (day 14) injections, as measured by endpoint titers, to directly compare the potentially maximal responses elicited by each regimen[38] (Figure 4b; Figure S5, Supporting Information). Noticeably, at this early time point, poly (I:C) adjuvanted RBD formulated in 6% and 12% gels induced robust RBD-specific IgG titers, while one bolus injection elicited minimal titers. IgG titers elicited by one bolus injection were 11.4- and 17.2-fold lower in comparison with 6% and 12% gels, respectively. Only after two bolus injections were significant RBD-specific titers observed, though still 3.3- and 4.9- fold lower than the 6% and 12% gels, respectively. These results confirmed that RBD-based subunit vaccine was poorly immunogenic, but RBD-poly (I:C) preparation was active.[11,37,39] Most strikingly, similar RBD-specific titers were observed between mice receiving three bolus injections and those receiving hydrogels, indicating the capability of the hydrogel scaffolds to significantly improve RBD immunogenicity by slow release. Together, these data demonstrated that the hydrogel formulations, after a single administration, rapidly induced superior humoral immune responses in 14 days that were comparable to three bolus injections that span 28 days.

As distinct IgG isotypes may function quite differently in SARS-CoV-2 pathogenesis, we profiled the titers of the major IgG subtypes elicited by different vaccine formulations.[40] Interestingly, the hydrogel formulations elicited both IgG1 and IgG2b, suggesting polarization of the humoral responses toward a mixed T_H1–T_H2 phenotype, while three bolus injections primarily induced IgG1, indicating a T_H2 dominant humoral response[38]

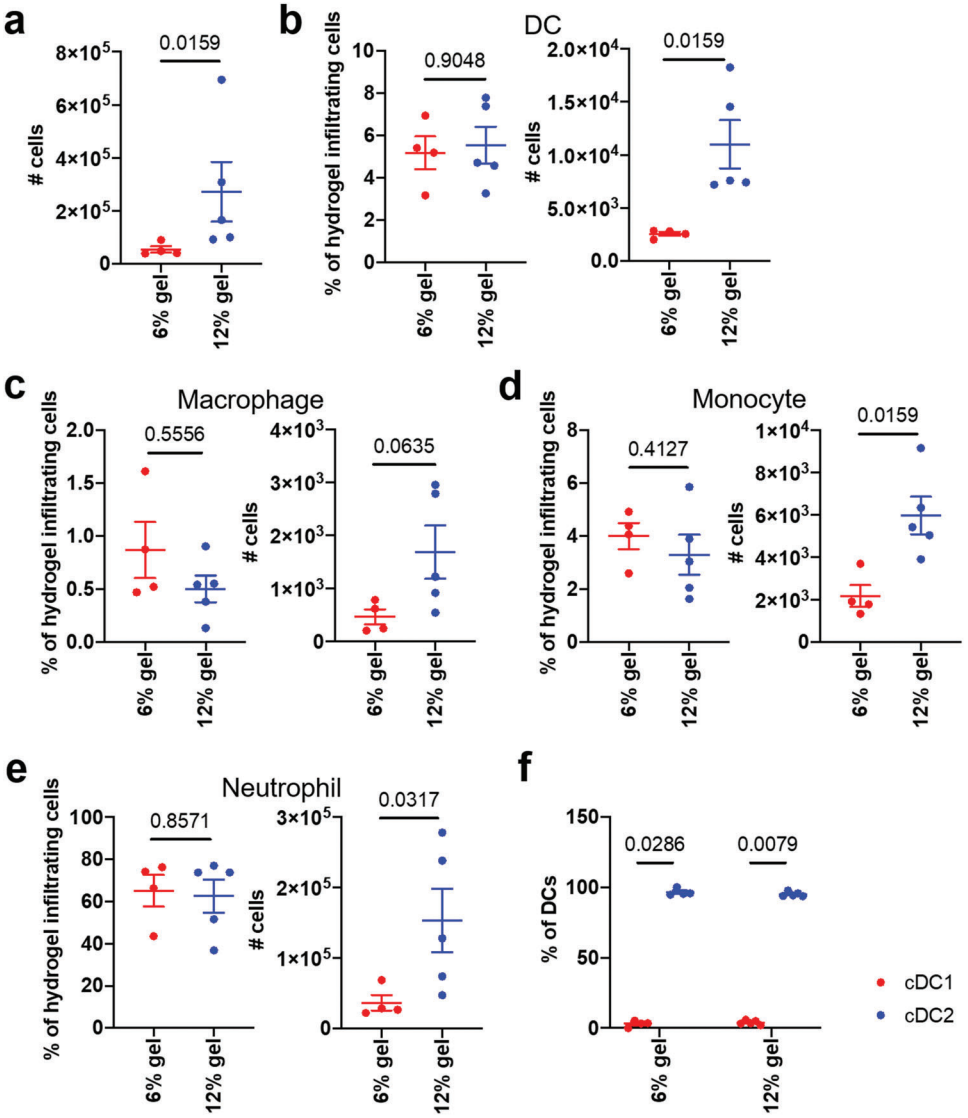

Figure 3. The hydrogel scaffolds serve as a local inflammatory site to recruit innate immune cells. Mice were immunized on day 0, and the hydrogels were collected on day 14 after immunization ($n = 4$ mice for 6% gel, and $n = 5$ mice for 12% gel). a) Absolute counts of total immune cells infiltrating into the hydrogels. b–e) Frequency and absolute counts of different innate immune cell subsets in the hydrogel scaffolds, including DC b), macrophage c), monocyte d), and neutrophil e). f) Frequency of each DC subset of the total DCs in the hydrogel scaffolds. Data were presented as mean ± S.E.M., and *p*-values were determined by a two-tailed t test.

(Figure 4c). Negligible IgG2c titers were observed in these three regimens. To our knowledge, this is the first report that prolonged delivery of immunogen by hydrogel scaffolds shifted the isotypes of serum IgG elicited. It is possible that the unique hydrogel chemistry (triple hydrogen bonding clusters) resulted in altered interactions with recruited APCs, therefore modified their functions, e.g., secretion of different cytokines, which in turn caused T_H1–T_H2 balanced humoral responses. However, whether the mixed T_H1–T_H2 type humoral response resulted from sustained release of poly (I:C) adjuvanted RBD or from the special chemistry of the hydrogel scaffolds needs further investigation.

We next performed a longitudinal analysis of RBD-specific serum IgG titers elicited by various RBD-poly (I:C) formulations (Figure 4d; Table S3, Supporting Information). Distinct titer dynamics were observed for bolus injections and administration of the hydrogel scaffolds. For one bolus injection, a delayed RBD-specific humoral immune response was noted at day 28 after immunization, though IgG titers rapidly decayed on day 42. As expected, a significant boost of RBD-specific titers was seen on day 28 (14 days after the second injection) for two bolus injections, and similarly on day 28 and day 42 (14 days after the second and third injections, respectively) for three bolus injections. The two regimens showed titers waning on days 63 and 77, respectively. In contrast, RBD-specific titers induced by 6% and 12% gels remained high through day 63, which started to wane slightly on day 77. On day 100 post-immunization, they reached similar levels as on day 14. These data not only further indicate the capability of the hydrogel formulations to induce rapid and robust humoral

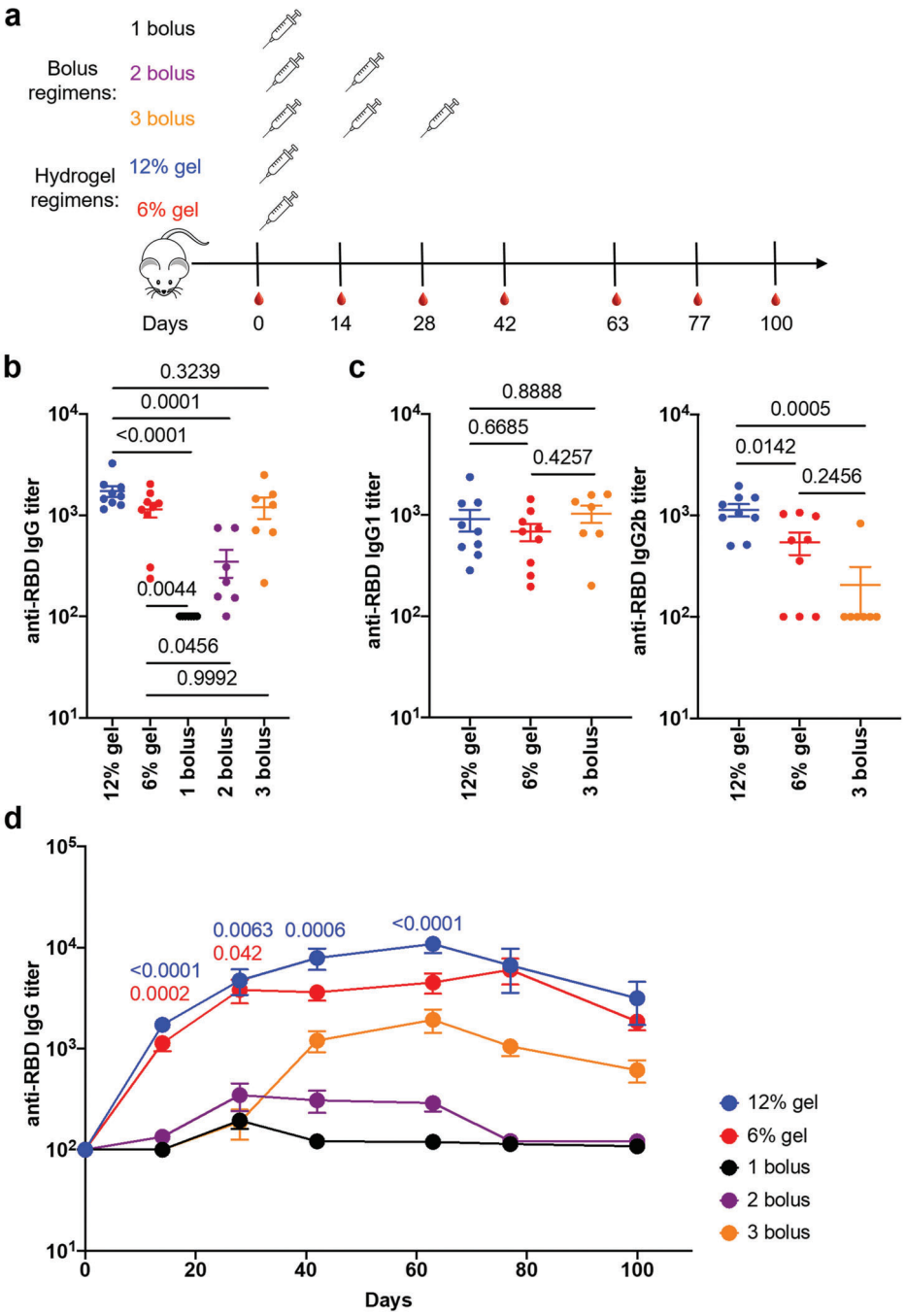

Figure 4. Hydrogel formulations drive strong and durable SARS-CoV-2 RBD-specific humoral immune responses. a) Timeline of mice immunization and blood sampling. For all groups, mice were immunized on day 0 (n = 7 mice for 1, 2, and 3 bolus, n = 9 mice for 6% and 12% gels). The 2 and 3 bolus groups were boosted on day 14, and day 14 and 28, respectively. Blood was harvested on day 0, 14, 28, 42, 63, 77, and 100 for RBD-specific titer determination. b) RBD-specific serum IgG titers 14 days after 1 bolus, the second of 2 bolus, the third of 3 bolus, 6% gel, and 12% gel injections. c) RBD-specific serum IgG1 and IgG2b titers 14 days after the third of 3 bolus, 6% gel, and 12% gel injections. d) RBD-specific serum IgG titers over time. p values were calculated for 6% gel and 12% gel vs three bolus injections, respectively. In (b–d), mean ± S.E.M. was shown, and one-way ANOVA with Turkey's post hoc test was conducted. Titers below 10^2, were displayed as 10^2.

immune responses against RBD, but also suggest that they enabled more durable responses, both of which are desirable for vaccination.

To uncover the mechanisms underlying the enhanced anti-RBD humoral immune responses mediated by the hydrogel scaffolds, we investigated GC dynamics in draining inguinal lymph nodes (LN), during one bolus, and 6% and 12% gel regimens. GCs in secondary lymphoid organs are where affinity maturation and class switching of antigen-specific B cells happen; therefore, they are pivotal for induction of high-quality humoral

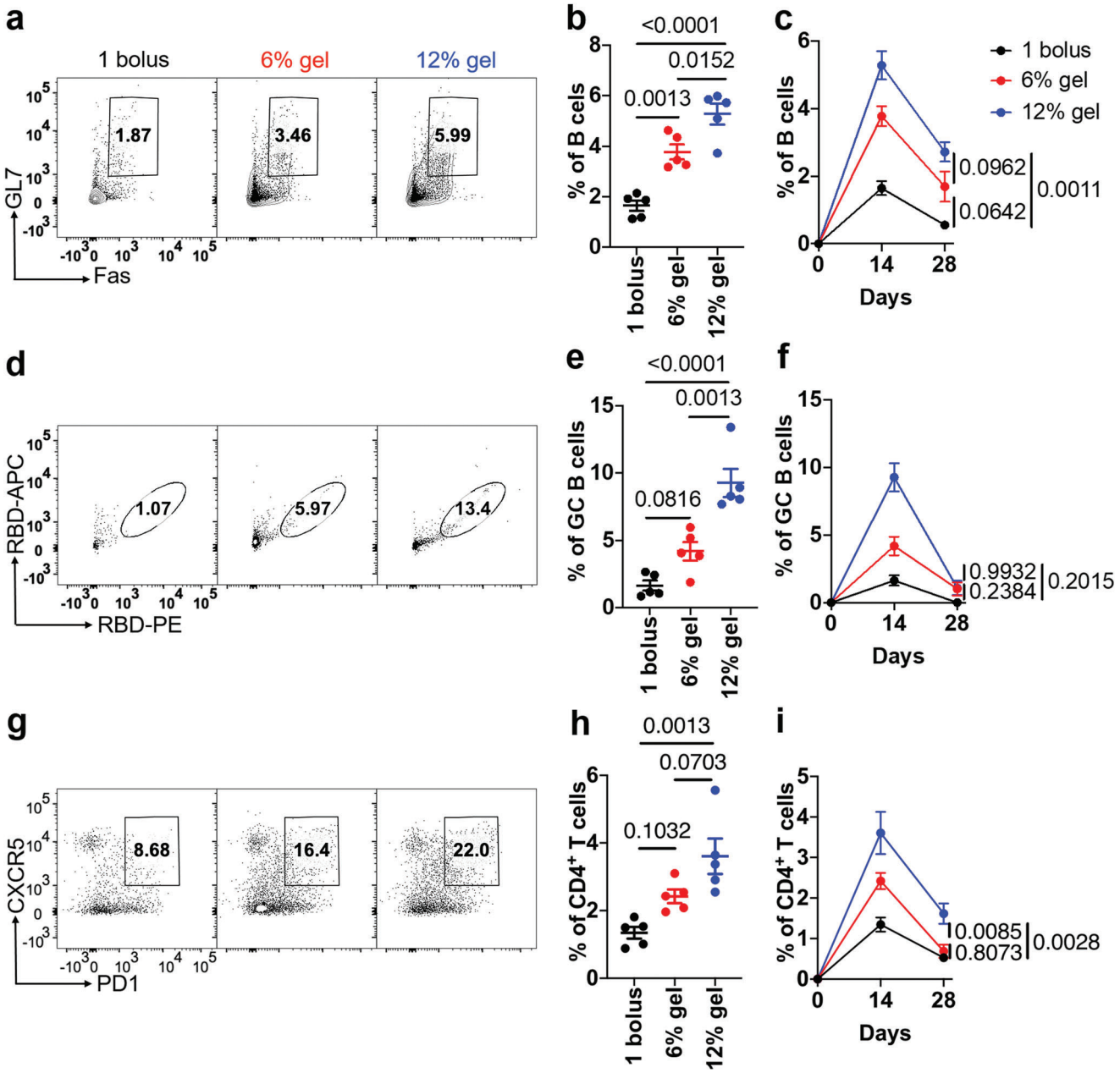

Figure 5. Hydrogel vaccine formulations promote GC responses. Mice were immunized on day 0, and the inguinal LNs were collected on day 14 (a, b, d, e, g, h) and 28 (c, f, i) for analysis. a) Representative FACS plots of GC B cells, defined as live $CD45^+CD19^+Fas^+GL7^+$ cells. b) Frequency of GC B cells as defined in (a). c) Kinetics of GC B cell frequency. d–f) Representative FACS plots of RBD-specific GC B cells d), their frequency on day 14 e), and their kinetics over the course of vaccination f). RBD-specific GC B cells are defined as live $CD45^+CD19^+Fas^+GL7^+RBD\text{-}PE^+RBD\text{-}APC^+$ cells. g–i) Representative FACS plots of T_{FH} cells g), their frequency on day 14 h), and their kinetics i). Cells were pre-gated on live $CD45^+CD3^+CD4^+CD44^{hi}CD62L^-$ cells. For each immunization group, $n = 5$ mice were analyzed on day 14 and 28, respectively. In (b,c,e,f,h,i), data were presented as mean ± S.E.M., and p values were determined by one-way ANOVA with Turkey's post hoc test.

immune responses.[41] Multiple studies have reported positive correlations between robust humoral responses and strong GC reactions elicited by SARS-CoV-2 mRNA vaccines.[42,43] We first evaluated GC B cells, defined as Fas^+GL7^+ B cells, using flow cytometry over the course of vaccination (Figure S6 and Table S4, Supporting Information). In line with augmented RBD-specific IgG titers induced by the hydrogel formulations, both 6% and 12% gels elicited elevated GC B cell populations on day 14 post-immunization (**Figure 5**a,b; Figure S8a, Supporting Information). On day 28 when GC B cells shrank for all three formulations, the 6% and 12% gels still showed higher GC B cell numbers than the single injection (Figure 5c; Figure S8b, Supporting Information). As it is established that not all GC B cells are antigen specific, we sought to determine whether the hydro-

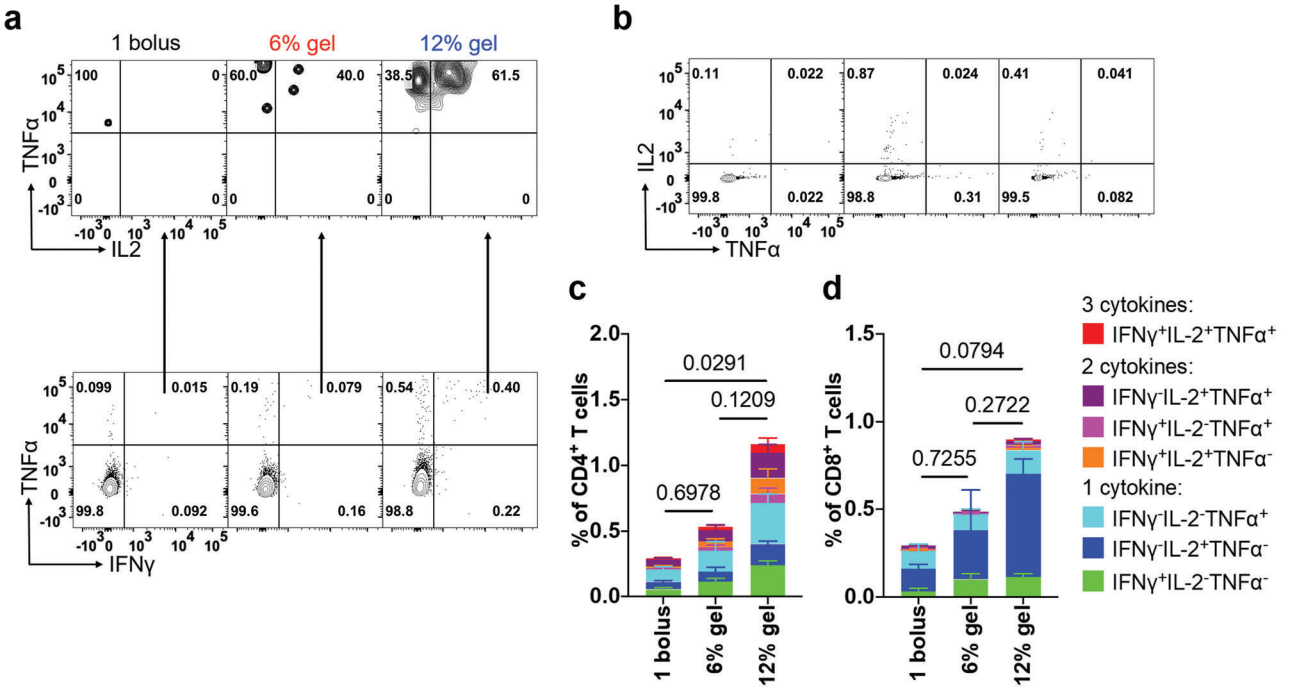

Figure 6. Hydrogel formulations induce SARS-CoV-2 RBD-specific T cell immune responses. Mice were immunized on day 0, and the spleens were harvested, processed to single cells, and stimulated with SARS-CoV-2 RBD peptide pools 14 days post-immunization. a) Representative FACS plots of IFN-γ^+TNF-α^+ CD4$^+$ T cells, which were further gated to characterize IFN-γ^+IL-2$^+$TNF-α^+ cells. b) Representative FACS plots of IL-2$^+$TNF-α^+ CD8$^+$ T cells, as determined by intracellular staining. c,d) Frequencies of each category of cells in CD4$^+$ and CD8$^+$ subsets. $n = 5$ mice per immunization group were analyzed. mean ± S.E.M. was shown, and one-way ANOVA with Turkey's post hoc test was conducted.

gel formulations increased RBD-specific GC B cells.[41,44] To this end, we generated two fluorescent RBD probes by conjugating biotinylated RBD with streptavidin-PE and streptavidin-APC,[45–47] respectively, and detected RBD-specific GC B cells by flow cytometry (Figure 5d). Indeed, on day 14 post-immunization, both 6% and 12% gels showed elevated RBD-specific GC B cells (Figure 5e; Figure S8c, Supporting Information). The kinetics of RBD-specific GC B cells was comparable to that of total GC B cells, which also contracted at day 28 (Figure 5f; Figure S8d, Supporting Information).

T_{FH} cells are key regulators of GC responses, as they select for B cells expressing affinity-matured antigen-specific receptors in GC light zones (LZ).[41,48] We thus characterized T_{FH} dynamics post-vaccination, measured by flow cytometry as CD4$^+$CD44^{hi}CD62L$^-$ cells that expressed T_{FH} signatures PD-1 and CXCR5 (Figure 5g; Figure S7 and Table S5, Supporting Information). In agreement with potent GC B cell induction by the hydrogel formulations, they promoted robust generation of T_{FH} cells 14 days after immunization (Figure 5h and Figure S8e, Supporting Information). The kinetics of T_{FH} cells mirrored GC B cells, which waned on day 28 (Figure 5i; Figure S8f, Supporting Information). Importantly, similar to the case of GC B cells, the hydrogel formulations still displayed higher T_{FH} induction on day 28 (Figure 5i; Figure S8f, Supporting Information).

We further performed Spearman correlation between day 14 RBD-specific serum titers and different GC cellular components to confirm the importance of enhanced GC reactions to boosted titers by the hydrogel formulations. As anticipated, total and RBD-specific GC B cell numbers strongly correlated with serum IgG titers on day 14 (Figure S9a,b, Supporting Information). A robust correlation between T_{FH} cell numbers and RBD-specific IgG titers was also noted (Figure S9c, Supporting Information). Additionally, on day 14 post-immunization, significant correlations between GC B cell numbers and T_{FH} cell numbers, and between RBD-specific GC B cell numbers and T_{FH} cell numbers were observed (Figure S9d,e, Supporting Information), again indicating the critical function of T_{FH} cells in GC responses. Taken together, these GC characterization data suggested that the hydrogel formulations elicited potent GC responses, consistent with elevated serum anti-RBD IgG titers.

Though humoral immune responses are essential to block virus–host interactions, cellular immune responses are also indispensable for clearance of infected host cells.[49–52] Multiple studies have demonstrated the critical importance of early T cell responses and T cell memory for protection against SARS-CoV-2, and mRNA vaccines have been shown to potently elicit T_H1 responses that minimize the risk of vaccine-associated enhanced respiratory disease.[53–56] To determine whether the hydrogel formulations induced RBD-specific T cell responses, we examined splenic T cells from immunized mice after in vitro stimulation with a RBD peptide pool together with CD28 co-stimulation by intracellular cytokine staining (Figure S10 and Table S6, Supporting Information). At 14 days post-immunization, both hydrogel formulations robustly elicited antigen-specific, polyfunctional CD4$^+$ and CD8$^+$ T cells that expressed T_H1 cytokines (interferon-γ (IFN-γ), tumor necrosis factor-α (TNF-α), and interleukin-2 (IL-2)) (**Figure 6**; Figure S11, Supporting Information). These results indicated the capability

of the hydrogel formulations to elicit robust T_H1-biased cellular responses.

3. Conclusion

In conclusion, we developed hydrogel formulations for sustained delivery of poly (I:C) adjuvanted SARS-CoV-2 RBD, with the aim of enhancing the immunogenicity of RBD for vaccination against COVID-19. Multiple SARS-CoV-2 vaccines have been approved for emergency use, though with distinct limitations.[8] For example, mRNA vaccines BNT162b2 and mRNA1273 rely heavily on cold chain logistics for distribution and storage, which may be difficult to be deployed in certain less developed areas.[8] Adenovirus-vectored vaccines ChAdOx1 nCoV-19 and Ad26.COV 2.S may cause rare, but severe thrombotic thrombocytopenia.[8,9] Together with inactivated virus vaccine CoronaVac, they all require non-trivial manufacture.[8] In contrast, subunit vaccines may provide an alternative route for massive vaccination against COVID-19 with less demanding manufacture and more flexibility to focus immune responses on protective epitopes, such as the RBD described in this work.[8] However, subunit vaccines, including RBD-based ones, are often poorly immunogenic, which requires multiple administrations to achieve protection.[11,37,39] Multivalent display of RBD on nanoparticles have been proven to improve its immunogenicity,[11,13,37] but this requires genetic fusion of RBD with other self-assembling units or chemical conjugation with preassembled nanoparticles, which may result in low immunogen yield or inactivation of RBD upon decoration on nanoparticles. On the other hand, sustained delivery of subunit vaccines using microneedles, osmotic pumps, or hydrogels have been demonstrated to enhance humoral immunity.[29,57–59] Crotty and coworkers even found that prolonged release of HIV envelop trimers resulted in B cell repertoire modulation that targeted a more diverse array of epitopes.[59] These results indicate the potential of sustained delivery of SARS-CoV-2 RBD to elicit potent humoral immunity.

We hypothesized that augmented interactions between the hydrogel scaffold and RBD resulted in sustained release, which could robustly enhance humoral immunity. To identify the optimal chemistry for RBD loading, we performed in silico analysis of the interactions between the RBD and side chains of various injectable hydrogel polymers used for protein delivery, and identified the combination of $–NH_2$ and three –OH in *p*(APMA-THMA) as the one with the lowest interacting energy. Using this hydrogel scaffold, we showed that after loading of poly (I:C) adjuvanted RBD vaccine, the scaffold was injectable and maintained its solid-like structure after injection, which prolonged cargo release in comparison with bolus vaccine injections. The sustained delivery of poly (I:C) adjuvanted RBD vaccine indeed translated to enhanced and long-lasting humoral immunity, demonstrated by augmented anti-RBD serum IgG titers. Interestingly, unlike bolus injections that resulted in T_H2-type antibody responses (high IgG1 titers and low IgG2b titers), the hydrogel formulations skewed toward a mixed T_H1–T_H2 type antibody responses (high IgG1 and IgG2b titers). Though the underlying mechanisms of this polarization warrant further investigation, mixed T_H1–T_H2 type responses may be desirable to achieve optimal protection against SARS-CoV-2.[40]

The biodegradability of the hydrogel scaffolds prompted us to investigate whether immune cells could infiltrate into the scaffolds. A comprehensive immunophenotyping identified infiltration of multiple immune cell subsets, with robust number of DCs and monocytes. These results suggested that the hydrogel scaffolds served as a local inflammatory niche for APC infiltration and T cell priming. In agreement with these results, we also observed elevated GC reactions in draining inguinal LNs. Hence, the extended release of adjuvanted RBD, together with the creation of a local inflammatory microenvironment, better mimics SARS-CoV-2 encounters during natural infections, which enhances the immune responses against RBD.

As cellular immunity is also critical for protection against SARS-CoV-2,[53–56] eliciting optimal T cell responses is another aim for vaccination. We found that the hydrogel formulations robustly elicited type 1, RBD-specific, polyfunctional T cells. Together with the mixed T_H1–T_H2 type humoral responses, the hydrogel formulations may potentially provide a desirable route for vaccination to avoid vaccine-associated enhanced respiratory disease.[40]

One limitation of the current study is that we did not characterize immune memory, especially RBD-specific memory B cells, elicited by the hydrogel vaccination system. Immune memory is one of the key mechanisms by which vaccines offer protection against future pathogenic infection.[38] Hence, eliciting effective immune memory is another long-sought-after aim for sustained delivery systems of vaccines. Our preliminary analysis in a small cohort of mice showed that the 12% gel elicited an increase of memory B cells. However, we are currently performing more detailed analysis of the immune memory induced by the hydrogel vaccine.

In summary, this study presents a sustained delivery system for SARS-CoV-2 RBD that enables elicitation of antigen-specific humoral immune responses that are of similar magnitude as the responses induced by three bolus injections. Our hydrogel scaffold system may provide an inexpensive and robust approach for large scale vaccination against SARS-CoV-2 and other endemic and pandemic pathogens.

4. Experimental Section

Materials: Natural, food grade sodium hyaluronate (hyaluronic acid) powder (HA) was purchased from Prescribed for Life, MW 1.8 million Daltons. N-(3-aminopropyl)methacrylamide hydrochloride (APMA) was purchased from Accela. Sodium dodecyl sulfate (SDS), picrylsulfonic acid solution (TNBS, 5% (w/v) in H_2O), ammonium persulfate (APS), and N-[Tris(hydroxymethyl)methyl]acrylamide (THMA), acetone, and HCl were purchased from Sigma-Aldrich.

In Silico Screening: AutoDockTools 1.5.6 Software, AutoDock Vina Software, and PyMOL version 0.99 Software were used for in silico screening. AutoDockTools 1.5.6. provided an accessible interface for processing ligands and targets. Polar hydrogen atoms and Gasteiger charges can also be easily added. Molecular docking was then carried out by AutoDock Vina. Visualization and analysis of protein-ligand complexes were finally performed using PyMOL. The crystal structure of the SARS-CoV-2 RBD (PDB ID: 7BWJ, chain E) was used as "receptor" for the docking calculations. All water molecules were removed followed by the addition of non-polar hydrogens. The respective amino acids were defined as flexible. Gasteiger charges were added and rotatable bonds were assigned using AutoDockTools. The chemical structures for each ligand were drawn with ChemAxon,

converted to MOL format, followed by processing with AutoDockTools 1.5.6 to assign Gasteiger charges before merging non-polar hydrogens and setting torsional bonds. Grid box center and grid dimensions (40 × 40 × 40 Å, grid spacing: 1.0 Å) were determined via AutoDockTools and transferred to the AutoDock Vina configuration file for docking calculation. The docking parameters including "modes" "exhaustiveness" and "energy_range" were set to "100", "20," and "3", respectively.

Synthesis of p(APMA-THMA): *p*(APMA-THMA) was synthesized and purified using previously reported methods.[31] APS initiator (23 mg, 0.1 mmol), THMA (728 mg, 4.16 mmol), and APMA (185 mg, 1.04 mmol) were dissolved in 6 mL of deionized (DI) water by stirring under a nitrogen atmosphere at room temperature (RT). The free radical polymerization reaction was then initiated by increasing the temperature to 60 °C. The reaction mixture was stirred at 60 °C for 1 h and then at 70 °C for an additional 12 h. *p*(APMA-THMA) was precipitated from the final reaction mixture using acetone, and then redissolved in water and dialyzed against water (Spectra/Pore, molecular weight cut off (MWCO) of 3500) for 4 days. The dialyzed polymer solution was lyophilized and reconstituted with water to achieve desired concentrations for hydrogel preparation. The degree of substitution (DS) of APMA in *p*(APMA-THMA) was found using a 2,4,6-trinitrobenzenesulfonic acid (TNBS) assay.

TNBS Assay: A TNBS assay for the determination of free amines was used to calculate the degree of substitution of APMA in the polymer according to a previously reported method.[31] Briefly, samples were incubated in a 0.01% TNBS solution (0.01 M sodium bicarbonate buffer, pH 8.5) for 2 h at 37 °C. Samples were then treated with HCl (1 M) and SDS (10%) to stop the TNBS reaction. The APMA monomer was incubated and processed under the same conditions and was used to generate a standard curve. The absorbance of the samples was read at 335 nm on a SpectraMax M5 microplate reader. The DS of APMA was calculated to be 15.7%.

Hydrogel Preparation: Hydrogels with 6% and 12% (wt/wt) solid contents were prepared by mixing amounts of hyaluronic acid (HA) and *p*(APMA-THMA) corresponding to a 1:1 ratio of primary amines of APMA to carboxyl groups of HA. The solutions were mixed with a spatula, mildly centrifuged to remove bubbles from mixing, and then loaded into a syringe.

Rheological Testing: Frequency sweeps over an angular frequency range of 1 to 100 rad s^{-1} were conducted with a strain of 0.1%. Storage and loss moduli (MPa) were plotted against angular frequency (rad s^{-1}), with both axes on a logarithmic scale. Flow ramp measurements with a shear rate range of 0.01–100 s^{-1} were conducted to observe the effects of shear rate on viscosity. Viscosity (Pa s) was plotted against shear rate (s^{-1}), with both axes on a logarithmic scale. Step-shear measurements were taken to demonstrate the injectability of the hydrogels. The hydrogels underwent two cycles of alternating high shear (100 s^{-1}) and low shear (0.5 s^{-1}). Each step, either high or low shear, was 50 s. All measurements were taken at a temperature of 37 °C to simulate rheological behavior in vivo and utilized a 20.0 mm aluminum Peltier plate. All data was analyzed using TA Instruments Trios software and plotted using GraphPad Prism.

Mice: 6–8-weeks-old C57BL/6J mice were purchased from the Jackson Laboratories and used for immunization. All experiments were conducted under the protocol approved by Cornell University's Institutional Animal Care and Use Committee (IACUC).

RBD and Poly (I:C): SARS-CoV-2 RBD was produced as previously described.[60] Briefly, Expi293 cells (Gibco, A14527) at the density of 3 × 10^6 viable cells mL^{-1} were transfected with pcDNA3-SARS-CoV-2-S-RBD-8his vector (Addgene, 145145) encoding the codon optimized RBD using ExpiFectamine 293 tranfection kit (Gibco, A14524). The supernatant was harvested 6 days after transfection, sterile-filtered and subsequently loaded onto a customized Ni Sepharose excel column (Cytiva). RBD was eluted with phosphate buffered saline (PBS), pH 7.4, supplemented with 500 × 10^{-3} M imidazole, and buffer exchanged to PBS, pH 7.4 and concentrated using 10 kD Amicon centrifugal filter units (Millipore Sigma, UFC901024). RBD concentration was measured using Nanodrop, and its integrity was confirmed by SDS-PAGE and western blot with rabbit-anti-RBD polyclonal antibodies (Sino Biological, 40592-T62). RBD was then aliquoted, flask frozen, and stored in −80 °C until use.

For preparation of RBD-PE and RBD-APC probes for RBD-specific GC B cell detection, RBD was biotinylated using EZ-Link Sulfo-NHS-LC-Biotin (Thermo Scientific, A39257) per the manufacturer's instructions, and complexed with Streptavidin-PE (eBioscience, 12-4317-87) and Streptavidin-APC (eBioscience, 17-4317-82).

Poly (I:C) was purchased from Millipore Sigma (P1530).

In Vivo Hydrogel Degradation and RBD Release: RBD was labeled with Cy5 NHS ester (Abcam, ab146454) at a molar ratio of 1:8 for 4 h at RT per the manufacturer's instructions to aim for 1:1 molar ratio of RBD:Cy5. After labeling, excess Cy5 dye was removed with Zeba Spin Desalting columns, 7 K MWCO (Thermo Scientific, 89882). 30 µg Cy5 conjugated RBD was premixed with 100 µL hydrogel, and subcutaneously injected into C57BL/6 mice on the back. Immediately after implantation and 1, 7, 14, and 21 days post-injection, the gels were retrieved and weighed for degradation measurement. After weighing, the gels were homogenized in 200 µL PBS, pH 7.4 with the plunger of 1 mL syringe, and the fluorescence was read at 649 nm excitation and 666 nm emission using a BioTek plate reader. The fluorescence of the empty gels in PBS was also measured. After correcting for the hydrogel background fluorescence, RBD fluorescence at each time point was normalized to the fluorescence immediately after injection to calculate residual RBD in the gel. Non-linear regression was performed in GraphPad Prism 9 to characterize RBD release half-life.

RBD Antigenicity Analysis: 30 µg Cy5 labeled RBD was premixed with 100 µL 12% hydrogel, and incubated in 300 µL PBS, pH 7.4 with 20% mouse serum at 37 °C with 120 rpm for 6 days. On days 1, 2, 4, and 6, 100 µL media was retrieved, and 100 µL fresh media was supplemented. For determination of RBD concentration in the media, 50 µL fivefold serially diluted media from each time point and unmanipulated Cy5-RBD diluted in fresh media starting from 100 µg mL^{-1} was added to 96-well plates, and their fluorescence was read at 649 nm excitation and 666 nm emission using a BioTek plate reader. Released RBD concentration in the media was calculated using the standard curve built from unmanipulated Cy5-RBD as reference.

Sandwich ELISA was used to probe the structural integrity of released Cy5-RBD in the media. Briefly, 50 µL fivefold serially diluted media from each time point and unmanipulated Cy5-RBD diluted in fresh media starting from 10 µg mL^{-1} was added to 96-well flat bottom high binding plates (Corning, 3590) pre-coated with rabbit-anti-RBD polyclonal antibodies for RBD capture. After 1 h incubation at RT, 1:5000 diluted rabbit-anti-6× His HRP antibody (Jackson Immunoresearch Laboratories, 300-035-240) was added for RBD detection.

Absorbance at 450 nm from sandwich ELISA was normalized to RBD concentration in the media and reported.

Immunization: For one bolus injection, 30 µg RBD and 50 µg poly (I:C) were diluted in 100 µL PBS, pH 7.4 and subcutaneously injected on the back of mice. For two bolus injections, mice were primed with 15 µg RBD and 25 µg poly (I:C) diluted in 100 µL PBS, pH 7.4 and boosted with the same dose 14 days later. For three bolus injections, mice were primed with 10 µg RBD and 17 µg poly (I:C) diluted in 100 µL PBS, pH 7.4 and boosted with the same dose 14 and 28 days post-priming, respectively.

For administration of the hydrogel formulations, 30 µg RBD and 50 µg poly (I:C) were premixed with 100 µL hydrogel, and subcutaneously injected on the back of mice.

Sample Collection and Processing: 14 to 100 days after immunization, mice were anesthetized, and blood was collected from the orbital sinus with capillary tubes. After coagulation for 30 min at RT, the blood was centrifuged at 13 000 × *g* for 15 min, after which the supernatant (serum) was harvested and stored at −20 °C.

For collection of inguinal LNs, spleens, and hydrogel scaffolds, mice were euthanized, and the respective organs or hydrogel scaffolds were harvested and placed immediately in cold RPMI 1640 medium (Gibco, A1049101) supplemented with 10% HI-FBS (R&D Systems, S11150H), and 1% Penicillin-Streptomycin (Gibco, 15140122). Organs or hydrogel scaffolds were mechanically digested, and red blood cells were lysed using ACK lysing buffer (Gibco, A10492). Cells were then filtered through 70 µm cell strainers (Corning, 352350) to obtain single cell suspensions, which were directly used for culture or staining.

Enzyme-Linked Immunosorbent Assay (ELISA): 96-well flat bottom high binding plates were coated with 50 µL of 1 µg mL^{-1} RBD protein in PBS, pH 7.4 at 4 °C overnight (o/n). Plates were washed with PBS, pH 7.4 supplemented with 0.05% Tween-20 (PBST) and blocked with 2% BSA in PBS (blocking buffer) for 2 h at RT. Threefold serially diluted serum samples starting from 1:100 dilution in blocking buffer was incubated for 1 h at RT. After washing with PBST, 1:5000 diluted AffiniPure goat anti-mouse IgG (Jackson Immunoresearch Laboratories, 115-005-166) were incubated for 1 h at RT. After washing with PBST, 1-Step Ultra TMB-ELISA substrate solution (Thermo Scientific, 34028) was incubated for 10 min at RT, and the reaction was stopped with 2 M H_2SO_4. Absorbance was read at 450 nm using a BioTek plate reader.

RBD-specific endpoint titers were calculated as the reciprocal dilutions where OD450 was greater than the average of blanks plus three times the standard deviation.

Flow Cytometry: Single cell suspensions of inguinal LNs were incubated with Ghost Dye UV450 at 4 °C for 30 min. After washing with cold FACS buffer (PBS, pH 7.4, 2% HI-FBS, 2×10^{-3} M EDTA), cells were blocked with TruStain FcX plus antibody (BioLegend, 1566040) at 4 °C for 10 min and stained with the antibody cocktails for GC B cells (Table S3, Supporting Information) and T_{FH} cells (Table S4, Supporting Information) at 4 °C for 30 min, respectively. Cells were washed with FACS buffer, fixed with 4% PFA at 4 °C for 10 min, and stored at 4 °C until acquisition.

For single cell suspensions of spleens, 10^6 cells were resuspended in RPMI 1640 supplemented with 10% HI-FBS, 1% Penicillin–Streptomycin, and 55×10^{-6} M 2-mercaptoethanol (Gibco, 21985-023), and stimulated with 1.5 µg mL^{-1} RBD peptide pool (JPT, PM-WCPV-S-RBD) and 2.5 µg mL^{-1} anti-CD28 antibody (eBioscience, 16-0281-86) in 96-well U-bottom tissue-culture-treated plates at 37 °C for 1 h. After adding Brefeldin A solution (BioLegend, 420601), cells were incubated at 37 °C for another 5 h. Cells incubated with DMSO for 6 h and with activation cocktail (BioLegend, 423301) for 5 h were used as a negative and positive control, respectively. After stimulation, cells were washed with cold PBS, stained with Ghost Dye UV450, and Fc blocked. After staining with the surface antibody cocktail (Table S5, Supporting Information), cells were fixed and permeabilized with cytofix/cytoperm fixation/permeablization kit (BD Biosciences, 554714). Cells were stained with the intracellular antibody cocktail (Table S5, Supporting Information) at 4 °C for 30 min and washed. After fixation with 4% cold PFA, they were stored at 4 °C until acquisition.

Single cell suspensions from the hydrogel samples were stained similarly as those of inguinal LNs, except that a different antibody cocktail (Table S6, Supporting Information) was used. When absolute counts of cells were required, precision count beads (BioLegend, 424902) were added to the samples.

All samples were acquired on a FACSymphony A3 and data was analyzed with Flowjo 10.7.1.

Statistical Analysis: All statistical analysis was performed with GraphPad Prism 9. One-way ANOVA with Turkey's post hoc test or two-tailed t test was used to determine statistical significance for comparison of multiple or two groups, respectively. Correlations were determined using Spearman's rank coefficient with 95% confidence interval.

Supporting Information

Supporting Information is available from the Wiley Online Library or from the author.

Acknowledgements

J.C. and B.W. contributed equally to this work. This work was partially supported by Cornell COVID-19 seed grant (B.W.) and the Hartwell Foundation (M.M.). This work made use of the Cornell Center for Materials Research Shared Facilities which are supported through the NSF MRSEC program (DMR-1719875). Cornell Flow Cytometry Facility is thanked for access to FACSymphony A3.

Conflict of Interest

The authors declare no conflict of interest.

Data Availability Statement

The data that supports the findings of this study are available in the supplementary material of this article. The other data that support the findings of this study are available from the corresponding author upon reasonable request.

Keywords

cellular immunity, germinal center, humoral immunity, injectable hydrogel scaffolds, severe acute respiratory syndrome coronavirus 2 receptor binding domain, sustained release, vaccines

Received: August 18, 2021
Revised: October 26, 2021
Published online: November 16, 2021

[1] E. M. Abrams, S. J. Szefler, *Lancet Respir. Med.* **2020**, *8*, 659.
[2] H. F. Florindo, R. Kleiner, D. Vaskovich-Koubi, R. C. Acurcio, B. Carreira, E. Yeini, G. Tiram, Y. Liubomirski, R. Satchi-Fainaro, *Nat. Nanotechnol.* **2020**, *15*, 630.
[3] S. Su, L. Y. Du, S. B. Jiang, *Nat. Rev. Microbiol.* **2021**, *19*, 211.
[4] J. A. Grobler, A. S. Anderson, P. Fernandes, M. S. Diamond, C. M. Colvis, J. P. Menetski, R. M. Alvarez, J. A. T. Young, K. L. Carter, *Cell Host Microbe* **2020**, *28*, 638.
[5] K. S. Park, X. Q. Sun, M. E. Aikins, J. J. Moon, *Adv. Drug Delivery Rev.* **2021**, *169*, 137.
[6] Y. T. Dong, T. Dai, Y. J. Wei, L. Zhang, M. Zheng, F. F. Zhou, *Signal Transduction Targeted Ther.* **2020**, *5*, 237.
[7] T. T. Ye, Z. F. Zhong, A. Garcia-Sastre, M. Schotsaert, B. G. De Geest, *Angew. Chem., Int. Ed.* **2020**, *59*, 18885.
[8] F. Krammer, *Nature* **2020**, *586*, 516.
[9] K. Y. Lai, S. Y. Au, K. M. Fong, P. Y. I. Choi, S. Eichinger, T. E. Warkentin, A. Greinacher, *N. Engl. J. Med.* **2021**, *384*, 2092.
[10] J. Y. Chung, M. N. Thone, Y. J. Kwon, *Adv. Drug Delivery Rev.* **2021**, *170*, 1.
[11] A. A. Cohen, P. N. P. Gnanapragasam, Y. E. Lee, P. R. Hoffman, S. S. Ou, L. M. Kakutani, J. R. Keeffe, H. J. Wu, M. Howarth, A. P. West, C. O. Barnes, M. C. Nussenzweig, P. J. Bjorkman, *Science* **2021**, *371*, 735.
[12] Y. F. Kang, C. Sun, Z. Zhuang, R. Y. Yuan, Q. B. Zheng, J. P. Li, P. P. Zhou, X. C. Chen, Z. Liu, X. Zhang, X. H. Yu, X. W. Kong, Q. Y. Zhu, Q. Zhong, M. Xu, N. S. Zhong, Y. X. Zeng, G. K. Feng, C. W. Ke, J. C. Zhao, M. S. Zeng, *ACS Nano* **2021**, *15*, 2738.
[13] X. C. Ma, F. Zou, F. Yu, R. Li, Y. C. Yuan, Y. W. Zhang, X. T. Zhang, J. Y. Deng, T. Chen, Z. Song, Y. D. Qiao, Y. K. Zhan, J. Liu, J. S. Zhang, X. Zhang, Z. L. Peng, Y. Z. Li, Y. T. Lin, L. T. Liang, G. W. Wang, Y. S. Chen, Q. E. Chen, T. Pan, X. He, H. Zhang, *Immunity* **2020**, *53*, 1315.
[14] J. Chen, Y. Zou, C. Deng, F. H. Meng, J. Zhang, Z. Y. Zhong, *J. Controlled Release* **2017**, *259*, e65.
[15] Y. S. Gao, K. Peng, S. Mitragotri, *Adv. Mater.* **2021**, *33*, 2006362.
[16] Y. J. Jiang, J. Chen, C. Deng, E. J. Suuronen, Z. Y. Zhong, *Biomaterials* **2014**, *35*, 4969.
[17] M. D. G. Hughes, B. S. Hanson, S. Cussons, N. Mahmoudi, D. J. Brockwell, L. Dougan, *ACS Nano* **2021**, *15*, 11296.
[18] J. Chen, Y. Zou, C. Deng, F. H. Meng, J. Zhang, Z. Y. Zhong, *Chem. Mater.* **2016**, *28*, 8792.

[19] J. H. He, Z. X. Zhang, Y. T. Yang, F. G. Ren, J. P. Li, S. J. Zhu, F. Ma, R. Q. Wu, Y. Lv, G. He, B. L. Guo, D. K. Chu, *Nano-Micro Lett.* **2021**, *13*, 80.
[20] H. X. Yang, X. L. Qin, H. Y. Wang, X. Zhao, Y. G. Liu, H. T. Wo, C. Liu, M. Nishiga, H. D. Chen, J. Ge, N. Sayed, O. J. Abilez, D. Ding, S. C. Heilshorn, K. Li, *ACS Nano* **2019**, *13*, 9880.
[21] Z. H. Li, S. Q. Hu, K. Cheng, *Acc. Chem. Res.* **2019**, *52*, 1687.
[22] S. McLaughlin, B. McNeill, J. Podrebarac, K. Hosoyama, V. Sedlakova, G. Cron, D. Smyth, R. Seymour, K. Goel, W. B. Liang, K. J. Rayner, M. Ruel, E. J. Suuronen, E. I. Alarcon, *Nat. Commun.* **2019**, *10*, 4866.
[23] L. L. Bu, J. J. Yan, Z. J. Wang, H. T. Ruan, Q. Chen, V. Gunadhi, R. B. Bell, Z. Gu, *Biomaterials* **2019**, *219*, 119182.
[24] M. Norouzi, B. Nazari, D. W. Miller, *Drug Discovery Today* **2016**, *21*, 1835.
[25] Y. Zhuang, X. Yang, Y. Li, Y. Chen, X. Peng, L. Yu, J. Ding, *ACS Appl. Mater. Interfaces* **2019**, *11*, 29604.
[26] F. Teodorescu, Y. Oz, G. Queniat, A. Abderrahmani, C. Foulon, M. Lecoeur, R. Sanyal, A. Sanyal, R. Boukherroub, S. Szunerits, *J. Controlled Release* **2017**, *246*, 164.
[27] B. B. Seo, M. R. Park, S. C. Song, *ACS Appl. Mater. Interfaces* **2019**, *11*, 15201.
[28] H. J. Noh, Y. W. Noh, M. B. Heo, E. H. Kim, S. J. Park, Y. I. Kim, Y. K. Choi, Y. T. Lim, *Small* **2016**, *12*, 6279.
[29] G. A. Roth, E. C. Gale, M. Alcantara-Hernandez, W. Luo, E. Axpe, R. Verma, Q. Yin, A. C. Yu, H. L. Hernandez, C. L. Maikawa, A. A. A. Smith, M. M. Davis, B. Pulendran, J. Idoyaga, E. A. Appel, *ACS Cent. Sci.* **2020**, *6*, 1800.
[30] M. O. Dellacherie, A. Li, B. V. Y. Lu, C. S. Verbeke, L. Gu, A. G. Stafford, E. J. Doherty, D. J. Mooney, *Adv. Funct. Mater.* **2020**, *30*, 2002448.
[31] J. Chen, D. Wang, L. H. Wang, W. J. Liu, A. Chiu, K. Shariati, Q. S. Liu, X. Wang, Z. Zhong, J. Webb, R. E. Schwartz, N. Bouklas, M. L. Ma, *Adv. Mater.* **2020**, *32*, 2001628.
[32] K. Sadtler, M. T. Wolf, S. Ganguly, C. A. Moad, L. Chung, S. Majumdar, F. Housseau, D. M. Pardoll, J. H. Elisseeff, *Biomaterials* **2019**, *192*, 405.
[33] K. Sadtler, K. Estrellas, B. W. Allen, M. T. Wolf, H. N. Fan, A. J. Tam, C. H. Patel, B. S. Luber, H. Wang, K. R. Wagner, J. D. Powell, F. Housseau, D. M. Pardoll, J. H. Elisseeff, *Science* **2016**, *352*, 366.
[34] J. K. Krishnaswamy, U. Gowthaman, B. Y. Zhang, J. Mattsson, L. Szeponik, D. Liu, R. Wu, T. White, S. Calabro, L. Xu, M. A. Collet, M. Yurieva, S. Alsen, P. Fogelstrand, A. Walter, W. R. Heath, S. N. Mueller, U. Yrlid, A. Williams, S. C. Eisenbarth, *Sci. Immunol.* **2017**, *2*, eaam9169.
[35] B. Wang, C. A. Kluwe, O. I. Lungu, B. J. DeKosky, S. A. Kerr, E. L. Johnson, J. Jung, A. B. Rezigh, S. M. Carroll, A. N. Reyes, J. R. Bentz, I. Villanueva, A. L. Altman, R. A. Davey, A. D. Ellington, G. Georgiou, *Sci. Rep.* **2015**, *5*, 13926.
[36] B. Wang, C. H. Lee, E. L. Johnson, C. A. Kluwe, J. C. Cunningham, H. Tanno, R. M. Crooks, G. Georgiou, A. D. Ellington, *mAbs* **2016**, *8*, 1035.
[37] A. C. Walls, B. Fiala, A. Schafer, S. Wrenn, M. N. Pham, M. Murphy, L. V. Tse, L. Shehata, M. A. O'Connor, C. B. Chen, M. J. Navarro, M. C. Miranda, D. Pettie, R. Ravichandran, J. C. Kraft, C. Ogohara, A. Palser, S. Chalk, E. C. Lee, K. Guerriero, E. Kepl, C. M. Chow, C. Sydeman, E. A. Hodge, B. Brown, J. T. Fuller, K. H. Dinnon, L. E. Gralinski, S. R. Leist, K. L. Gully, et al., *Cell* **2020**, *183*, 1367.
[38] A. J. Pollard, E. M. Bijker, *Nat. Rev. Immunol.* **2021**, *21*, 83.
[39] J. Y. Yang, W. Wang, Z. M. Chen, S. Y. Lu, F. L. Yang, Z. F. Bi, L. L. Bao, F. Mo, X. Li, Y. Huang, W. Q. Hong, Y. Yang, Y. Zhao, F. Ye, S. Lin, W. Deng, H. Chen, H. Lei, Z. Q. Zhang, M. Luo, H. Gao, Y. Zheng, Y. Q. Gong, X. H. Jiang, Y. F. Xu, Q. Lv, D. Li, M. N. Wang, F. D. Li, et al., *Nature* **2020**, *586*, 572.
[40] B. S. Graham, *Science* **2020**, *368*, 945.
[41] N. S. De Silva, U. Klein, *Nat. Rev. Immunol.* **2015**, *15*, 137.
[42] K. Lederer, D. Castano, D. G. Atria, T. H. Oguin, S. Wang, T. B. Manzoni, H. Muramatsu, M. J. Hogan, F. Amanat, P. Cherubin, K. A. Lundgreen, Y. K. Tam, S. H. Y. Fan, L. C. Eisenlohr, I. Maillard, D. Weissman, P. Bates, F. Krammer, G. D. Sempowski, N. Pardi, M. Locci, *Immunity* **2020**, *53*, 1281 .
[43] J. S. Turner, J. A. O'Halloran, E. Kalaidina, W. Kim, A. J. Schmitz, J. Q. Zhou, T. Lei, M. Thapa, R. E. Chen, J. B. Case, F. Amanat, A. M. Rauseo, A. Haile, X. Xie, M. K. Klebert, T. Suessen, W. D. Middleton, P.-Y. Shi, F. Krammer, S. A. Teefey, M. S. Diamond, R. M. Presti, A. H. Ellebedy, *Nature* **2021**, *596*, 109.
[44] L. Mesin, J. Ersching, G. D. Victora, Germinal Center B Cell Dynamics, *Immunity* **2016**, *45*, 471.
[45] D. F. Robbiani, C. Gaebler, F. Muecksch, J. C. C. Lorenzi, Z. J. Wang, A. Cho, M. Agudelo, C. O. Barnes, A. Gazumyan, S. Finkin, T. Hagglof, T. Y. Oliveira, C. Viant, A. Hurley, H. H. Hoffmann, K. G. Millard, R. G. Kost, M. Cipolla, K. Gordon, F. Bianchini, S. T. Chen, V. Ramos, R. Patel, J. Dizon, I. Shimeliovich, P. Mendoza, H. Hartweger, L. Nogueira, M. Pack, J. Horowitz, et al., *Nature* **2020**, *584*, 437.
[46] G. E. Hartley, E. S. J. Edwards, P. M. Aui, N. Varese, S. Stojanovic, J. McMahon, A. Y. Peleg, I. Boo, H. E. Drummer, P. M. Hogarth, R. E. O'Hehir, M. C. van Zelm, *Sci. Immunol.* **2020**, *5*, 14.
[47] E. Seydoux, L. J. Homad, A. J. MacCamy, K. R. Parks, N. K. Hurlburt, M. F. Jennewein, N. R. Akins, A. B. Stuart, Y. H. Wan, J. L. Feng, R. E. Whaley, S. Singh, M. Boeckh, K. W. Cohen, M. J. McElrath, J. A. Englund, H. Y. Chu, M. Pancera, A. T. McGuire, L. Stamatatos, *Immunity* **2020**, *53*, 98 .
[48] S. Crotty, *Immunity* **2019**, *50*, 1132.
[49] E. S. Rosenberg, J. M. Billingsley, A. M. Caliendo, S. L. Boswell, P. E. Sax, S. A. Kalams, B. D. Walker, *Science* **1997**, *278*, 1447.
[50] L. M. Snell, I. Osokine, D. H. Yamada, J. R. De la Fuente, H. J. Elsaesser, D. G. Brooks, *Cell Rep.* **2016**, *16*, 3286.
[51] B. J. Laidlaw, J. E. Craft, S. M. Kaech, *Nat. Rev. Immunol.* **2016**, *16*, 102.
[52] J. F. Zhu, H. Yamane, W. E. Paul, *Annu. Rev. Immunol.* **2010**, *28*, 445.
[53] A. Grifoni, D. Weiskopf, S. I. Ramirez, J. Mateus, J. M. Dan, C. R. Moderbacher, S. A. Rawlings, A. Sutherland, L. Premkumar, R. S. Jadi, D. Marrama, A. M. de Silva, A. Frazier, A. F. Carlin, J. A. Greenbaum, B. Peters, F. Krammer, D. M. Smith, S. Crotty, A. Sette, *Cell* **2020**, *181*, 1489 .
[54] M. Jeyanathan, S. Afkhami, F. Smaill, M. S. Miller, B. D. Lichty, Z. Xing, *Nat. Rev. Immunol.* **2020**, *20*, 615.
[55] Y. C. Peng, A. J. Mentzer, G. H. Liu, X. Yao, Z. X. Yin, D. N. Dong, W. Dejnirattisai, T. Rostron, P. Supasa, C. Liu, C. Lopez-Camacho, J. Slon-Campos, Y. G. Zhao, D. I. Stuart, G. C. Paesen, J. M. Grimes, A. A. Antson, O. W. Bayfield, D. Hawkins, D. S. Ker, B. B. Wang, L. Turtle, K. Subramaniam, P. Thomson, P. Zhang, C. Dold, J. Ratcliff, P. Simmonds, T. de Silva, P. Sopp, et al., *Nat. Immunol.* **2020**, *21*, 1336.
[56] U. Sahin, A. Muik, I. Vogler, E. Derhovanessian, L. M. Kranz, M. Vormehr, J. Quandt, N. Bidmon, A. Ulges, A. Baum, K. E. Pascal, D. Maurus, S. Brachtendorf, V. Lorks, J. Sikorski, P. Koch, R. Hilker, D. Becker, A. K. Eller, J. Grutzner, M. Tonigold, C. Boesler, C. Rosenbaum, L. Heesen, M. C. Kuhnle, A. Poran, J. S. Z. Dong, U. Luxemburger, A. Kemmer-Bruck, D. Langer, et al., *Nature* **2021**, *595*, 572.
[57] A. V. Boopathy, A. Mandal, D. W. Kulp, S. Menis, N. R. Bennett, H. C. Watkins, W. Wang, J. T. Martin, N. T. Thai, Y. P. He, W. R. Schief, P. T. Hammond, D. J. Irvine, *Proc. Natl. Acad. Sci. USA* **2019**, *116*, 16473.
[58] H. H. Tam, M. B. Melo, M. Kang, J. M. Pelet, V. M. Ruda, M. H. Foley, J. K. Hu, S. Kumari, J. Crampton, A. D. Baldeon, R. W. Sanders, J. P. Moore, S. Crotty, R. Langer, D. G. Anderson, A. K. Chakraborty, D. J. Irvine, *Proc. Natl. Acad. Sci. USA* **2016**, *113*, E6639.

[59] K. M. Cirelli, D. G. Carnathan, B. Nogal, J. T. Martin, O. L. Rodriguez, A. A. Upadhyay, C. A. Enemuo, E. H. Gebru, Y. Choe, F. Viviano, C. Nakao, M. G. Pauthner, S. Reiss, C. A. Cottrell, M. L. Smith, R. Bastidas, W. Gibson, A. N. Wolabaugh, M. B. Melo, B. Cossette, V. Kumar, N. B. Patel, T. Tokatlian, S. Menis, D. W. Kulp, D. R. Burton, B. Murrell, W. R. Schief, S. E. Bosinger, A. B. Ward, et al., *Cell* **2019**, *177*, 1153.

[60] F. Amanat, D. Stadlbauer, S. Strohmeier, T. H. O. Nguyen, V. Chromikova, M. McMahon, K. J. Jiang, G. A. Arunkumar, D. Jurczyszak, J. Polanco, M. Bermudez-Gonzalez, G. Kleiner, T. Aydillo, L. Miorin, D. S. Fierer, L. A. Lugo, E. M. Kojic, J. Stoever, S. T. H. Liu, C. Cunningham-Rundles, P. L. Felgner, T. Moran, A. Garcia-Sastre, D. Caplivski, A. L. C. Cheng, K. Kedzierska, O. Vapalahti, J. M. Hepojoki, V. Simon, F. Krammer, *Nat. Med.* **2020**, *26*, 1033.